SAND2019-14455C

Hydrogen thermometry in aluminized propellant burns by hybrid fs/ps coherent anti-Stokes Raman scattering

Jonathan E. Retter[1], Daniel R. Richardson[2], and Sean P Kearney[3]
Sandia National Laboratories, Albuquerque, New Mexico 87815

A hybrid femtosecond/picosecond CARS instrument probed the Q-branch of molecular hydrogen in the multiphase plume of an aluminized solid propellant burn. A single 50 fs regenerative amplifier pumped an OPA and etalon, providing the Stokes and probe pulses respectively. The spectra were recorded at 1 kHz and fit to synthetic spectra to infer the gas rotational temperature. Recorded spectra required dynamic background corrections due to the intense emission of the propellant plume. Two different days of propellant burns were studied, with the lessons learned from nonresonant background issues with the first test applied to the second. For the second attempt, three burns were examined, with mean temperatures differing only by 30 K with a combined mean of 2574 K.

I. Introduction

Solid propellants remain useful for rocket propulsion, but not a lot is understood about the burn characteristics of these propellants. Aluminum is typically added to these propellants to increase the specific impulse and reduce any combustion instabilities, but in turn this creates a combined solid and gas phase burning region. This bright, high temperature, multi-phase plume requires many non-intrusive laser diagnostics to characterize the burn environment. Our lab has focused specifically on small benchtop burns of aluminized ammonium perchlorate hydroxyl terminated polybutadiene (AP/HTPB/AL) composites with an example burn image shown in Fig. 1. Previous holography and pyrometry measurements [1] of these propellants detailed aluminum particle size, velocity, and temperature, while nitrogen rotational coherent anti-Stokes Raman scattering (CARS) measurements [2] probed the gas-phase temperature in the plume.

Fig. 1 Example image of a propellant stick burn.

The work presented in this manuscript expands on the previous CARS measurements by probing the fuel species of hydrogen, appearing as isolated gaseous molecules by the decomposition of the HTPB binder, as a product of binder and AP reactions, and from radical recombination reactions [3]. By probing the fuel, as opposed to inert N_2, we are ensuring our measured temperature is directly involved in the chemical reaction and eliminating any spatial averaging with the surrounding cold air. We report rotational temperatures of the H_2 molecule by probing the Q-branch Raman transitions ($\Delta v = 1$, $\Delta J = 0$) by means of a now very common hybrid fs/ps CARS instrument, including the use of an etalon probe pulse [4,5].

[1] Postdoctoral Researcher, Engineering Sciences Center, AIAA Member
[2] Senior Member of the Technical Staff, Engineering Sciences Center, AIAA Senior Member
[3] Distinguished Member of the Technical Staff, Engineering Sciences Center, Associate Fellow AIAA

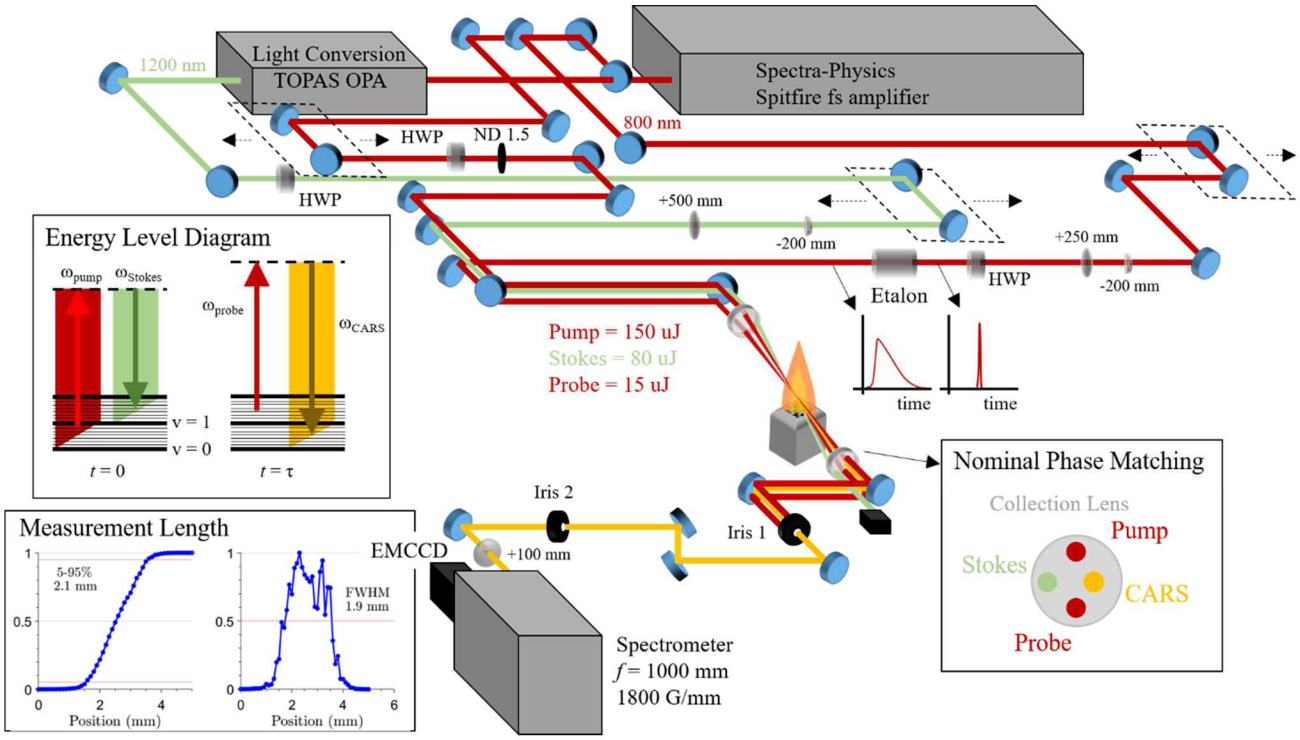

Fig. 2 Optical setup used for the H_2 thermometry, including inserts of the energy level diagram, the phase matching scheme, and the measurement length on both a FWHM and 5-95% basis.

II. Experimental Setup

A. Optical Setup

The optical setup for the hybrid fs/ps CARS system is shown in Fig. 2. A single fs amplifier (Spectra-Physics Spitfire Ace, 800 nm, 50 fs, 1 kHz, 11.3 mJ) acts as the source for all three beams in a BOXCARS phase matching [6] scheme seen as an insert on the bottom right of Fig. 2. The output energy of the amplifier is split using a series of beam splitters to regulate the energy to acceptable values for this fs CARS experiment. To generate a Stokes-shifted beam from the fundamental 800 nm to match the Q-branch of molecular hydrogen (~4160 cm^{-1}), 4 mJ is used to pump an OPA (Light Conversion TOPAS) which after a series of delay lines resulted in ~80 uJ of 1200 nm light at the focus. A separate ~1.5 mJ of 800 nm light acted as the pump pulse, traveling through a neutral density filter to regulate the pulse energy down to ~150 uJ at the focus. A filter was chosen in place of a waveplate and polarizer combination to avoid the generation of pulse trains in the thin film polarizer. Finally, another ~1.5 mJ of 800 nm pumped an angle-tuned air-spaced etalon (free spectral range ~30.27 cm^{-1}, finesse ~ 104 at 800 nm) to achieve a temporally longer, but relatively frequency narrow time-asymmetric pulse used as the probe pulse to allow for frequency isolation of the Raman peaks. The temporal shape of the probe pulse is used as an input to our spectral model and is displayed in Fig. 3, was obtained by recording the nonresonant signal generation in argon as a function of probe delay. The temporal resolution of 33.3 fs was at the limit of the delay stage capability. The beams were positioned such that 90% of the signal generation occurred within 2.1 mm.

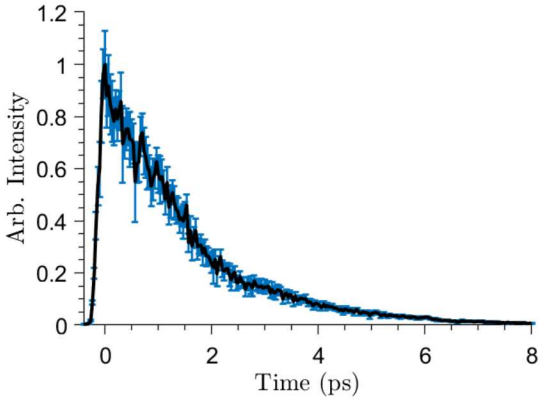

Fig. 3 Temporal profile of the probe pulse shaped by an etalon (blue = mean and standard deviation, black = mean)

B. Burn Timeline

To avoid optical complexity, the interaction volume of the three CARS beams was held constant in space and the propellant stick burned down and through the measurement region. Therefore, measurements later in time were also higher above the burning surface of the propellant stick. A cartoon of the burn timeline is featured in Fig. 4, detailing an actual photograph of the propellant stick, a single-shot detector image of the spectrum (or noise), and a cartoon of the beam height with respect to the propellant stick. For initial alignment, the center of the beam overlap in the beam propagating direction was found by translating a thin glass coverslip through the measurement volume while monitoring the nonresonant spectrum on the detector. Neutral density filters were positioned just before the beam crossing lens to equally decrease the energy from all 3 beams without altering the relative timing to prevent burning the coverslip at the focus. The coverslip was held at the position of maximum signal intensity, marking the center of the beam overlap. The propellant stick was mounted on a 3-axis translation stage to allow trivial positioning of the stick just below the glass coverslip. The coverslip was removed, but the neutral density filters remained in place while the propellant stick was translated up and into the beam crossing, such that the beams are hitting the propellant stick.

To begin the burn, we started the camera acquisition, pulled the neutral density filter allowing the full energy of the beams to hit the propellant stick, and activated the resistive heating element mounted to the stick which began the ignition process. The first several acquisitions of the detector were just the detector noise, as seen in the top left block of Fig. 4, but as the stick burned down, there was significant broadband emission from the plume recorded on the detector while the CARS beams were still hitting the propellant stick. As the beams first became clear of the solid propellant and could prepare/probe the gas, resonant hydrogen CARS spectra were clearly observable on the detector above the broadband emission. Initially, close to the burning surface, the measured spectra appeared colder, with relative populations shifted toward higher wavenumbers as opposed to later or higher in the burn where the spectra appear hotter with the lines biased towards lower wavenumbers (see the difference in the upper right block and lower left block of Fig. 4). Finally, at late times in the burn where the CARS beams are high off the burning surface, no resonant or broadband emission signal is observed, only the background of the CARS beams themselves. Each propellant stick was approximately 53.3 mm in length and took from 33-39 seconds to burn, resulting in an average burn rate of 1.49 mm/s. With the measurement system repetition rate of 1 kHz, this provides a spatial resolution of ~1.49 μm/laser shot.

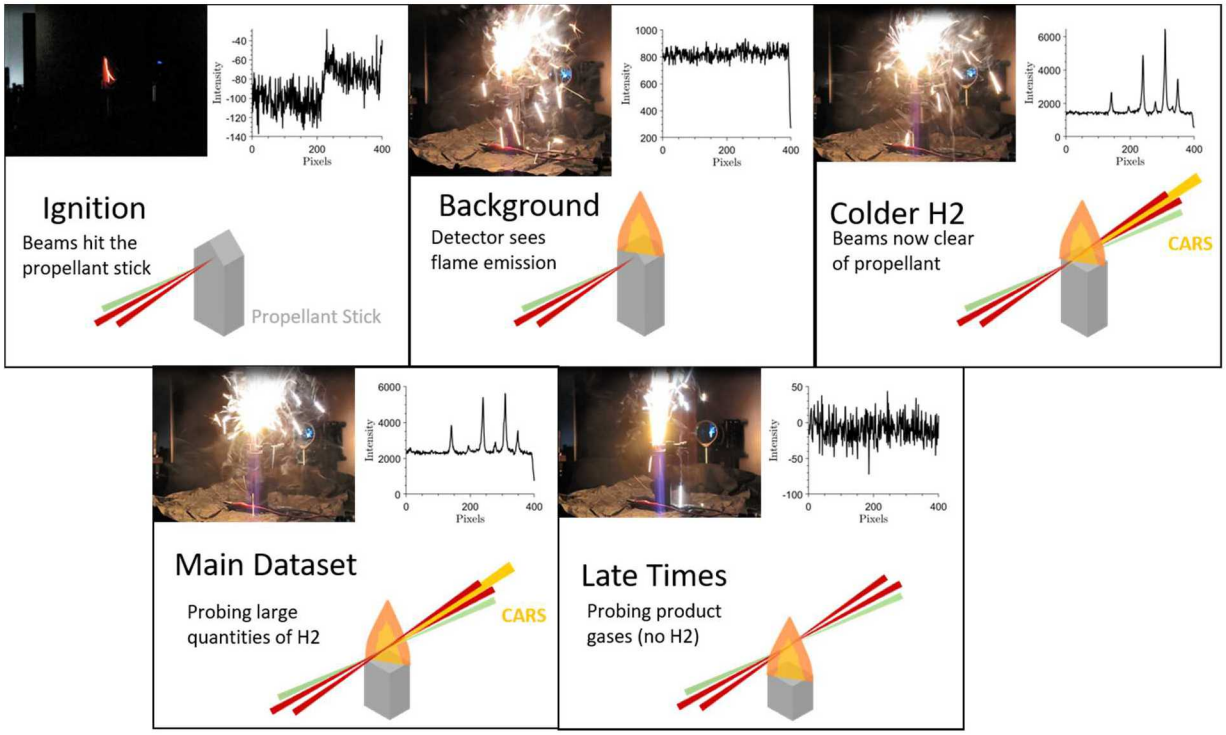

Fig. 4 Cartoon depiction of the propellant burn throughout the burning process.

III. Data Processing

All measured spectra were background subtracted and normalized by the nonresonant spectrum in argon to account for the limited bandwidth of the CARS pump/Stokes pulses. However, the relatively broadband emission of the propellant plume created issues with just a simple background correction, as from shot-to-shot for each 90 μs camera exposure, the detected broadband spectrum changed. Examples of single-shot raw spectra (black) along with the fitted dynamic background correction (shown in red) and the corresponding corrected signal (blue) are seen in Fig. 5.

The dynamic background correction consisted of a linear fit to the pixel values between the resonant spectral lines. Higher order fits were attempted but would lead to erroneous "corrections" that would bias the intensity of pixels over a resonant line. Linear fits proved effective for most resonant spectra, as just a simple baseline offset (Fig. 5a) was enough, and at times the broadband plume emission also provided gradients of intensity across the detector chip (Fig. 5b-c). However, as detailed in Fig. 5d, not every background was reasonably fit with a linear relationship. The corresponding corrected spectra would be thrown out in the fitting residual cutoff procedure discussed later.

We attempted to mitigate this broadband emission with spatial filtering, spectral filtering, and further time-gating the acquired CARS signal. The spatial filtering included 6 reflections off of 600 nm dichroic mirrors and two irises optimized to pass the nonresonant signal seen by eye on a business card in room air, but these precautions alone produced the plots seen in Fig. 5. We also tried further spectral filtering, but with the inexpensive filters on hand we lost too much resonant signal in the process. Finally, implementing a liquid crystal optical shutter was attempted to further time gate the acquired CARS signal, but the shutter would not work effectively at 1 kHz, the repetition rate of the laser. Therefore, we only performed spatial filtering of the CARS signal and tolerated the dynamic background correction, but there are opportunities to improve the spectral or temporal filtering in the future.

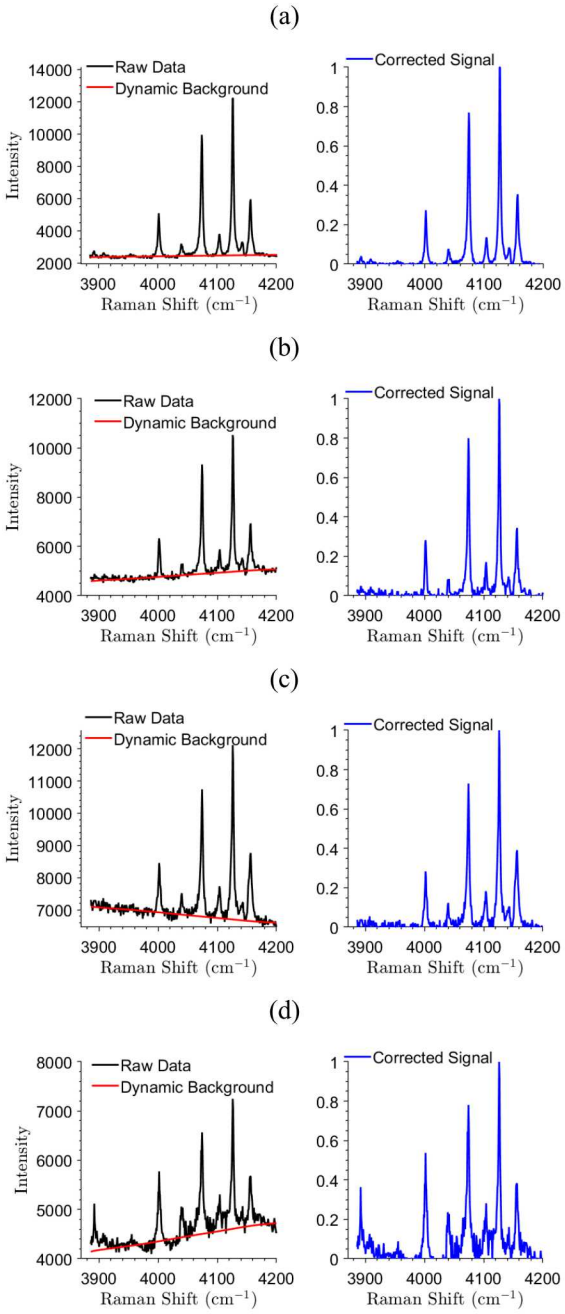

Fig. 5 Example dynamic background fits to different single shot spectra.

Another issue we faced was the change in preparation bandwidth with time evidenced by the change in the nonresonant spectrum with time. As mentioned previously, each raw spectrum after the appropriate background correction, was normalized by the nonresonant background to achieve the true spectral shape of the CARS signal. However, as the bandwidth of the overlapped pump/Stokes pulses changes, the required correction changes in time. Therefore, it is easy to record resonant spectra but not have the coinciding nonresonant correction factor for that moment in time. For the first set of propellant burns, we only recorded the nonresonant spectrum before and after the burns, with the results shown in Fig. 6a. While similar in structure, there is clearly different correction factors as a function of Raman shift, leading

to significant uncertainty as to which nonresonant spectra to use for each burn. The different corrections will result in different weights of relative rotational states, seen in Fig. (6a), and thus fits to different temperatures.

We believe this issue of the drifting nonresonant background was due to the quality of the Stokes pulse from the OPA. Cross correlations of the pump and Stokes pulses in argon displayed significant changes in the nonresonant spectra with delay of one pulse from the other, suggesting chirp in one or more of the pulses. If both femtosecond pulses were transform limited, a change in the timing between the preparation pulses would lead to spectra focusing, or optimization of certain spectral regions. However, we saw significant nonlinear variations with pump/Stokes timing which could not be explained by spectral focusing.

We believe this nonresonant issue also limited the precision floor of our instrument to 3% about the mean for signal-to-noise ratios over 75, while pure-rotational schemes utilizing a common pump/Stokes pulse originating from the femtosecond amplifier showed as low as 1% precision [7]. We attempted to mitigate this issue by pumping the OPA with lower pulse energy and with a longer pulse by carving bandwidth out of the OPA pump pulse with a filter, but neither method proved effective.

Our solution to this was to "bound" each set of resonant spectral acquisitions with nonresonant backgrounds recorded directly before and after each propellant burn to mitigate the "walking" of the effective bandwidth of the preparation pulses. Examples of these before and after nonresonant spectra are shown in Fig. 6b, which common colors (light versus dark) defining the measurements before and after burns. Each pair was reasonably similar, much more so than the before and after nonresonant signals from the precious attempt (Fig. 6a), so the average of the two was used as the normalization curve for all of the resonant spectra recorded for each burn.

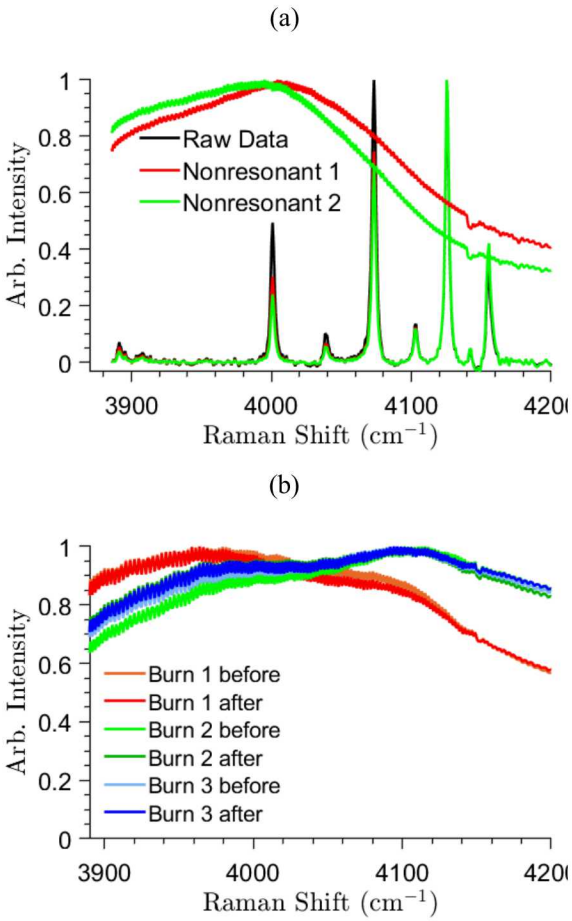

Fig. 6 Example of the nonresonant issues before and after the propellant burns.

A library of synthetic spectra was generated to fit the experimental spectra, where only the resonant Raman response, $\chi(t)$, for H_2 Q-branch transitions ($\Delta v = 1$, $\Delta J = 0$) is observed and is modeled as

$$\chi(t) \sim \sum_{\Delta v=1} \sum_{\Delta J=0} g_J \left| N_J (N_{v'} - N_v) \right| \cos(\omega_{v,J} t) \exp(-\Gamma_{v,J} t), \quad (1)$$

where g_J is the nuclear spin statistical weight term for each rotational (J) state, N_J and N_v are the thermally populated Boltzmann distributions for rotational and vibrational (v) levels where $v' = v + 1$, $\omega_{v,J}$ are the Raman frequencies [8], and $\Gamma_{v,J}$ are the corresponding collisional linewidths [9].

Once each spectrum was appropriately background corrected and normalized by the nonresonant background, they were fit to these libraries. Initially, two-dimensional fits of probe delay and temperature were performed to determine the actual probe delay of 2.66 ps utilizing the experimental probe temporal profile shown previously in Fig. 3. Then, the probe delay was fixed, and all spectra were fit for rotational temperatures of hydrogen alone. The fitting procedure allowed for horizontal and vertical shifts of the synthetically generated spectra with respect to the experimental, along with a horizontal scaling factor. The synthetic library was linearly interpolated over the temperature grid to determine the best fit to each experimental spectrum. The residual of each fit, shown in Fig. 7 by the black line for each subplot, was used as a filter to determine which fits were considered for actual analysis of the plume gas-phase temperature. As an example, the left column of Fig. 7 contains experimental spectra with fits deemed good enough to keep for analysis purposes while those in the right column were ignored.

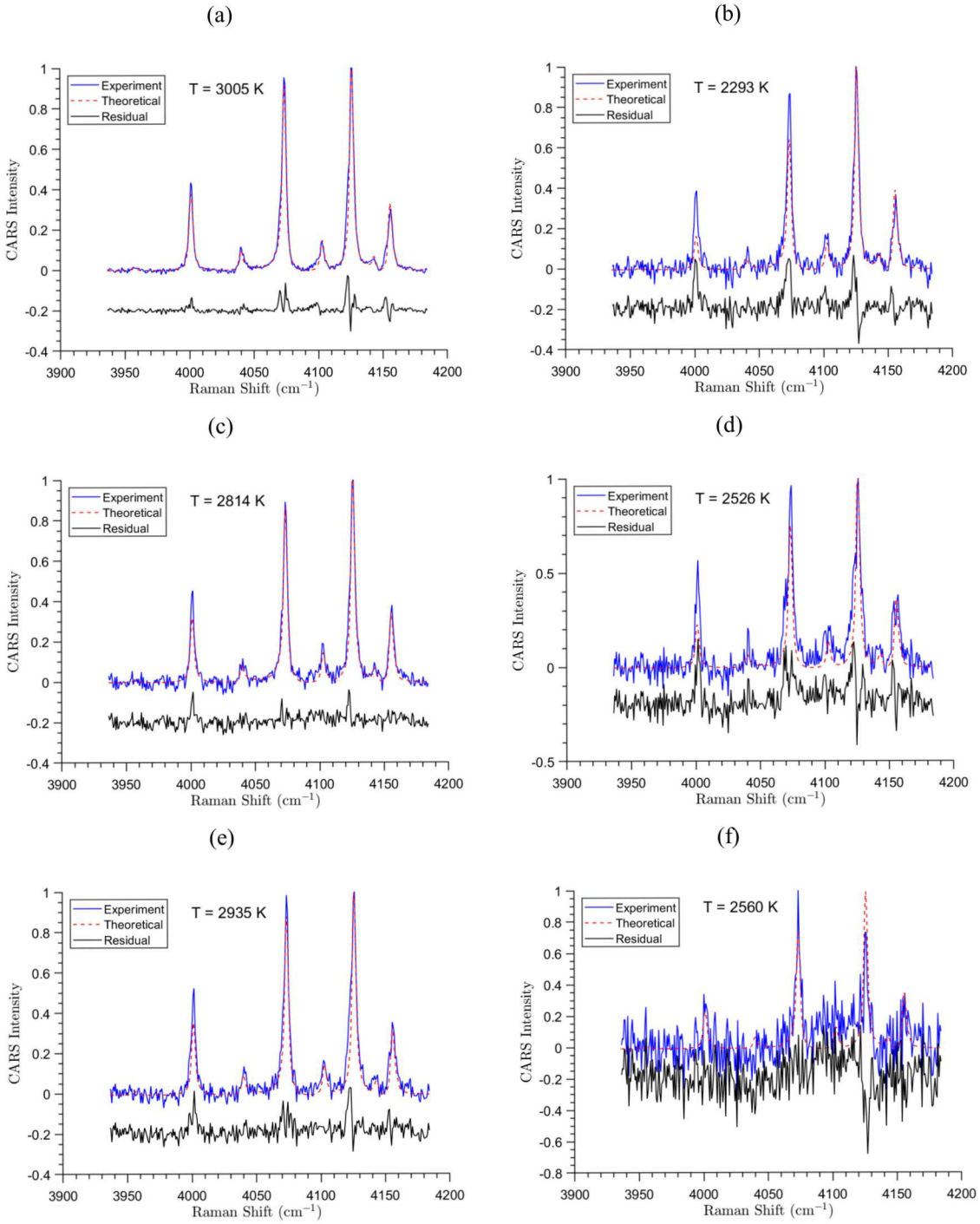

Fig. 7 Examples of retained spectra (left column) and spectra that are thrown out and not considered in the final dataset (right column). The corresponding residuals are as follows: (a) 2.7, (b) 10.9, (c) 6.1, (d) 17, (e) 9.3, and (f) 34.8.

IV. Results

A. Hencken Burner Measurements

To test our hydrogen rotational thermometry instrument, we probed a hydrogen-air flame stabilized on a Hencken burner. This canonical flame is known to closely match adiabatic equilibrium flame temperatures [7,10]. The results of the mean fitted temperature from 200 laser shots for equivalence ratios from 1.0-1.8 are displayed in Fig. 8 in comparison to theoretical hydrogen-air equilibrium predictions [11]. The error bars signify the standard deviation of the fitted temperature. Our measurements are systematically lower than the theoretical values, most likely due to some heat loss to the burner surface and thus a deviation of our burner from true adiabatic conditions. All measurements occurred as close to the burner surface as possible (~1 cm off the burner), and there was clear heating of the burner especially at higher equivalence ratios. With increasing signal-to-noise by increasing equivalence ratio corresponding to higher concentrations of hydrogen (specifically >1.3), our average measurements are within 5% of theory and approach a precision of 3% about the mean, providing confidence in our instrument and processing procedures to reasonably measure the gas rotational temperature. Higher equivalence ratios, with continuing increases in hydrogen concentration, were not feasible with our 2-inch square mesh burner and our available flow controllers.

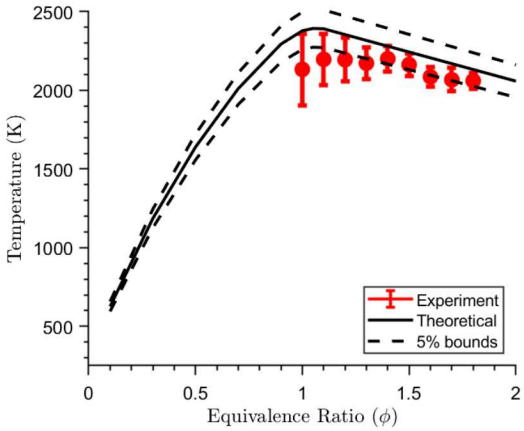

Fig. 8 Fitted mean temperatures and error bars of the standard deviation of 200 shots for equivalence ratios of 1.0-1.8 compared to adiabatic equilibrium.

B. Propellant Burn Measurements

Two days of propellant burns are presented in this section. The first set includes the uncertainty in the nonresonant background as shown previously in Fig. 6a. Histograms of all the resonant fits and those that met the residual cutoff defined in the previous section are shown in Fig. 9a and 9c, respectively, for four different propellant burns. The burns are listed in chronological order, thus as seen in the histograms the fitted temperatures increase in time from a mean of 2386 K to 2708 K from runs 1 to 4. This is not a real effect, as again the drifting nonresonant spectra, or effective bandwidth of the CARS system, caused measurements taken later in time to be biased hotter than they physically are. The propellant burns occurred once every 15-20 minutes, which is, unfortunately, plenty of time for the pump/Stokes pulses to drift in quality.

By bounding the resonant acquisition before and after each burn, the histograms of fitted temperatures all converge to a common mean as seen with all the spectral fits and those meeting the residual cutoff in Fig. 9b and 9d, respectively. The mean values of the three burns only differ by 30 K, with a mean temperature of 2574 K encompassing all three burns. The data retention rate was only ~32% on average for the 3 runs over the first 10 seconds of the burn, but as high as ~57% on average for the first second of each burn. At early times, dynamic background emission plagued the retention rate, while the low fuel concentration at late times prevented the acquisition of large quantities of high-quality spectra. Note that even with the difference in the nonresonant spectrum associated with each burn, seen in Fig. 6b, the final fitted temperatures all coincide, providing us confidence in our procedure and revealing how consistent these propellant burns are on average.

The coinciding running time-average burn temperature of 100 retained spectra for both days of propellant burns are shown in Fig. 10. Once again, those spectra contaminated with nonresonant uncertainty, Fig. 10a, display a wide range in measured temperature, while the fitted temperatures with bounded nonresonant spectra, Fig. 10b, show near identical behavior. Focusing on these results of Fig. 10b, there is a measurable temperature rise from just over 2200 K to over 2600 K just as the burning surface of the propellant passes the beam crossing. After this initial rise, the average measured temperature is nearly constant above 2500 K for the remainder of the burn time when resonant hydrogen signal is obtainable. These early colder measurements may be indicative of measurements in the vicinity of burning AP alone, known as a monopropellant flame, which aids in the thermal decomposition of the surrounding binder material, releasing molecular hydrogen into the plume for additional high-temperature reactions further from the burning surface.

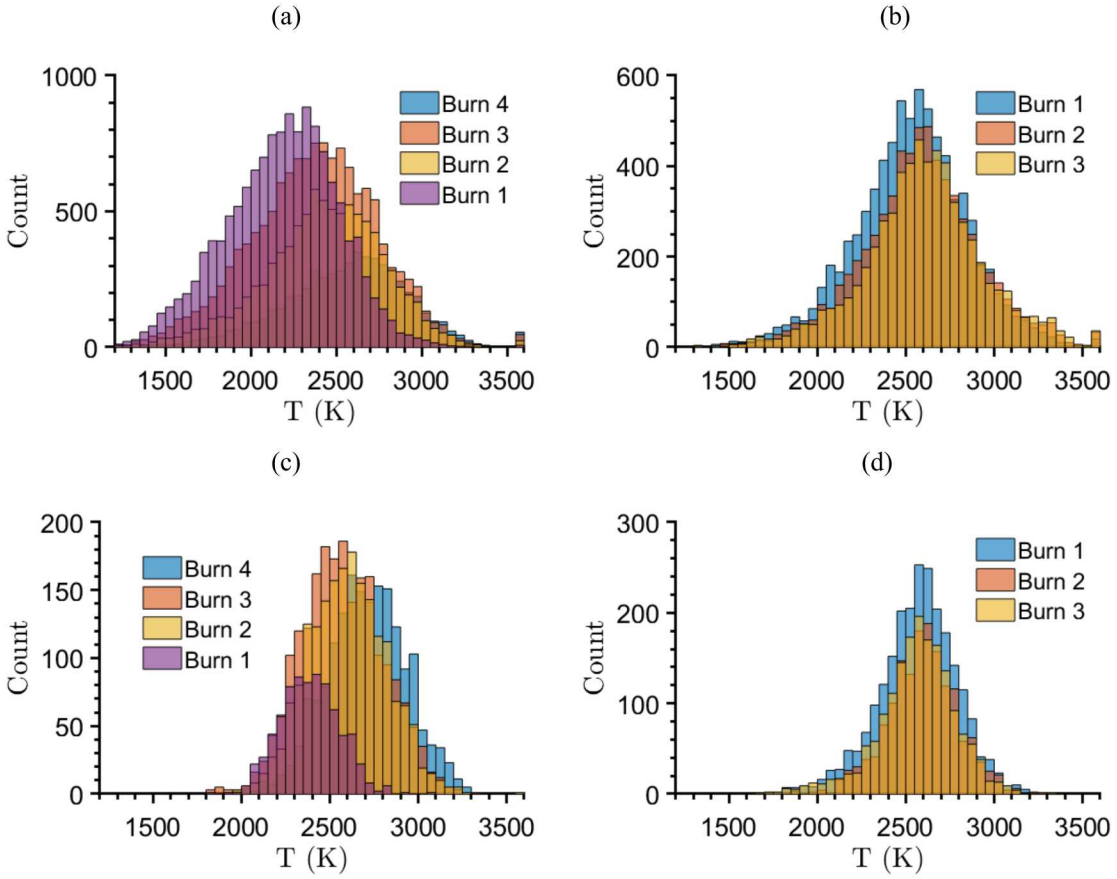

Fig. 9 Histograms from all spectra (top row) and only the retained spectra (bottom row) for two days of propellant burns. The histograms in (a) and (c) were contaminated with the uncertainty in the nonresonant background spectra, while those in (b) and (d) were not.

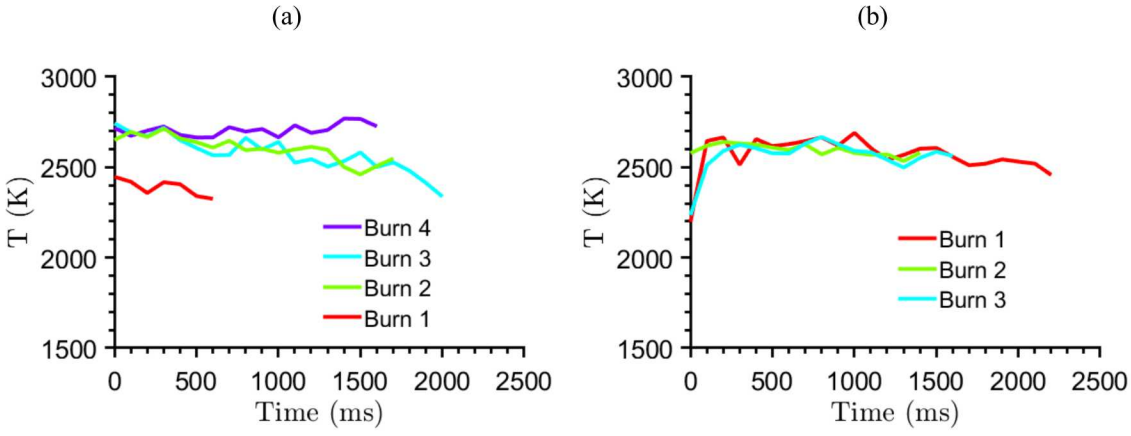

Fig. 10 Running time averages of 100 shots for (a) burns with nonresonant background uncertainty and (b) those without uncertainty.

V. Summary and Conclusions

A hydrogen Q-branch hybrid fs/ps CARS instrument was designed to probe the gas-phase plume of a burning solid propellant stick at local atmospheric pressure. The frequency and spatially isolated CARS signal was generated by an etalon-shaped time-asymmetric pulse probing a femtosecond pump/Stokes preparation in a BOXCARS configuration. Fitted temperatures to the measured resonant spectra in a canonical Hencken burner were accurate within 5% to theoretical adiabatic equilibrium predictions, with a precision approaching 3% for higher signal-to-noise spectra. Two days of propellant burns were examined, both of which required dynamic background corrections to the measured resonant spectra and great care in monitoring the nonresonant background in time. The three burns studied with corresponding bounded nonresonant spectra differed in mean temperature by only 30 K, with an overall mean of 2574 K. Future work may include parametric studies to examine how these temperature scale with physical size of the propellants and comparisons to other types of thermometry instruments applied to these propellant burns.

Acknowledgments

The authors would like to thank Howard L. Stauffacher, Sam M. Reardon, and Glen White for their efforts in preparing and handling the propellant. This paper describes objective technical results and analysis. Any subjective views or opinions that might be expressed in the paper do not necessarily represent the views of the U.S. Department of Energy or the United States Government. Sandia National Laboratories is a multimission laboratory managed and operated by National Technology & Engineering Solutions of Sandia, LLC, a wholly owned subsidiary of Honeywell International Inc., for the U.S. Department of Energy's National Nuclear Security Administration under contract DE-NA0003525.

References

[1] Chen, Y., Guildenbecher, D. R., Hoffmeister, K. N. G., Cooper, M. A., Stauffacher, H. L., Oliver, M. S., and Washburn, E. B. "Study of Aluminum Particle Combustion in Solid Propellant Plumes Using Digital In-Line Holography and Imaging Pyrometry." *Combustion and Flame*, Vol. 182, 2017, pp. 225–237. doi:10.1016/j.combustflame.2017.04.016.

[2] Kearney, S. P., and Guildenbecher, D. R. "Temperature Measurements in Metalized Propellant Combustion Using Hybrid Fs/Ps Coherent Anti-Stokes Raman Scattering." *Applied Optics*, Vol. 55, No. 18, 2016, p. 4958. doi:10.1364/ao.55.004958.

[3] Jeppson, M., Beckstead, M., and Jing, Q. "A Kinetic Model for the Premixed Combustion of a Fine AP/HTPB Composite Propellant." 1997. doi:10.2514/6.1998-447.

[4] Stauffer, H. U., Miller, J. D., Roy, S., Gord, J. R., and Meyer, T. R. "Communication: Hybrid Femtosecondpicosecond Rotational Coherent Anti-Stokes Raman Scattering Thermometry Using a Narrowband Time-Asymmetric Probe Pulse." *Journal of Chemical Physics*, Vol. 136, No. 11, 2012. doi:10.1063/1.3693669.

[5] Kearney, S., Scoglietti, D., and Kliewer, C. "Hybrid Fs/Ps Rotational CARS Temperature and Concentration Measurements Using Two Different Ps-Duration Probe Beams." No. January, 2013, pp. 1–12. doi:10.2514/6.2013-338.

[6] Eckbreth, A. C. "BOXCARS: Crossed-Beam Phase-Matched CARS Generation in Gases." *Applied Physics Letters*, Vol. 32, No. 7, 1978, pp. 421–423. doi:10.1063/1.90070.

[7] Kearney, S. P. "Hybrid Fs/Ps Rotational CARS Temperature and Oxygen Measurements in the Product Gases of Canonical Flat Flames." *Combustion and Flame*, Vol. 162, No. 5, 2014, pp. 1748–1758. doi:10.1016/j.combustflame.2014.11.036.

[8] Dabrowski, I. "The Lyman and Werner Bands of H2." *Canadian Journal of Physics*, Vol. 62, 1984, pp. 1639–1664.

[9] Kulatilaka, W. D., Hsu, P. S., Stauffer, H. U., Gord, J. R., and Roy, S. "Direct Measurement of Rotationally Resolved H2 Q -Branch Raman Coherence Lifetimes Using Time-Resolved Picosecond Coherent Anti-Stokes Raman Scattering." *Applied Physics Letters*, Vol. 97, No. 8, 2010, pp. 198–201. doi:10.1063/1.3483871.

[10] Hancock, R. D., Bertagnolli, K. E., and Lucht, R. P. "Nitrogen and Hydrogen CARS Temperature Measurements in a Hydrogen/Air Flame Using a near-Adiabatic Flat-Flame Burner." *Combustion and Flame*, Vol. 109, No. 3, 1997, pp. 323–331. doi:10.1016/S0010-2180(96)00191-5.

[11] McBride, B. J., and Gordon, S. "Computer Program for Calculation of Complex Chemical Equilibrium Compositions and Applications II. Users Manual and Program Description." *NASA Reference Publication 1311*, 1996.